A fluorescein tracer release experiment in the hydrothermally active crater of Vailulu'u volcano, Samoa

S. R. Hart,[1] H. Staudigel,[2] R. Workman,[1] A. A. P. Koppers,[2] and A. P. Girard[1]

Received 28 March 2002; revised 26 March 2003; accepted 17 April 2003; published 14 August 2003.

[1] On 3 April 2001, a 20 kg point source of fluorescein dye was released 30 m above the bottom of the active summit caldera of Vailulu'u submarine volcano, Samoa. Vailulu'u crater is 2000 m wide and at water depths of 600–1000 m, with the bottom 200 m completely enclosed; it thus provides an ideal site to study the hydrodynamics of an active hydrothermal system. The magmatically driven hydrothermal system in the crater is currently exporting massive amounts of particulates, manganese, and helium. The dispersal of the dye was tracked for 4 days with a fluorimeter in tow-yo mode from the U.S. Coast Guard icebreaker *Polar Sea*. Lateral dispersion of the dye ranged from 80 to 500 m d^{-1}; vertical dispersion had two components: a diapycnal diffusivity component averaging 21 cm^2 s^{-1}, and an advective component averaging 0.025 cm s^{-1}. These measurements constrain the mass export of water from the crater during this period to be $8^{+4.6}_{-1.3} \times 10^7$ m^3 d^{-1}, which leads to a "turnover" time for water in the crater of ~3.2 days. Coupled with temperature data from CTD profiles and Mn analyses of water samples, the power output from the crater is 610^{+350}_{-100} MW, and the manganese export flux is ~240 kg d^{-1}. The Mn/Heat ratio of 4.7 ng J^{-1} is significantly lower than ratios characteristic of hot smokers and diffuse hydrothermal flows on mid-ocean ridges and points to phase separation processes in this relatively shallow hydrothermal system. *INDEX TERMS:* 1045 Geochemistry: Low-temperature geochemistry; 3015 Marine Geology and Geophysics: Heat flow (benthic) and hydrothermal processes; 3094 Marine Geology and Geophysics: Instruments and techniques; 4568 Oceanography: Physical: Turbulence, diffusion, and mixing processes; *KEYWORDS:* dye tracer, hydrothermal, eddy diffusion, volcanic, Vailulu'u

Citation: Hart, S. R., H. Staudigel, R. Workman, A. A. P. Koppers, and A. P. Girard, A fluorescein tracer release experiment in the hydrothermally active crater of Vailulu'u volcano, Samoa, *J. Geophys. Res.*, *108*(B8), 2377, doi:10.1029/2002JB001902, 2003.

1. Introduction

[2] The fluxes of thermal and chemical discharge from submarine hydrothermal areas are important for understanding the total energetic and elemental fluxes to the oceans and the atmosphere. By far, the largest contributors to these fluxes are the hydrothermal vent fields on mid-ocean spreading ridges. Despite almost 25 years of intensive study, the hydrodynamics of these fields remain contentious and enigmatic. While estimates of the total power output of these fields are reasonably well constrained, and of the order 75 ± 45 MW per kilometer of ridge length [*Baker et al.*, 1996], the chemical fluxes are still poorly constrained. At issue is the partitioning of hydrothermal mass flow between the spectacular high-temperature "hot smokers" and the more diffuse "lukewarm springs" [*Schultz and Elderfield*, 1997]. Because the temperature of water/rock reaction strongly influences the chemistry of the reacted fluids, we cannot know the chemical fluxes until we know the partitioning of mass flow between hot smokers and diffuse springs. While a ratio of 1:10 is often cited for this [*Elderfield and Schultz*, 1996], we believe the uncertainty is very large.

[3] The principal difficulty in establishing this partitioning on ridge systems is the open ended "trough-like" topography in which most vent fields are situated. While the hot smoker mass fluxes are so robust as to be unaffected by ambient bottom currents, the diffuse flows are easily advected away by currents. Our discovery [*Hart et al.*, 2000] of an active hydrothermal system in the summit crater of the submarine volcano Vailulu'u, Samoa (Figure 1), provides an ideal natural laboratory to study the physics and hydrodynamics of hydrothermal systems. An understanding of this isolated system can give us insights into the more complicated systems on ridge crests. The summit crater on Vailulu'u is 2 km wide and 400 m deep, with the lower 200 m completely enclosed (Figure 2). The crater is very actively venting hydrothermal fluids, as witnessed by high particulate concentrations (up to 1.4 NTU (nephelometric turbidity units)), high Mn concentrations (up to 3.5 ppb) and high $^3He/^4He$ (up to 9.0 times atmospheric)[*Hart et al.*, 2000].

[4] To gain a basic understanding of the hydrothermal circulation in the crater, we performed a fluorescein dye

[1]Woods Hole Oceanographic Institution, Woods Hole, Massachusetts, USA.
[2]Scripps Institution of Oceanography, University of California, San Diego, La Jolla, California, USA.

0148-0227/03/2002JB001902$09.00

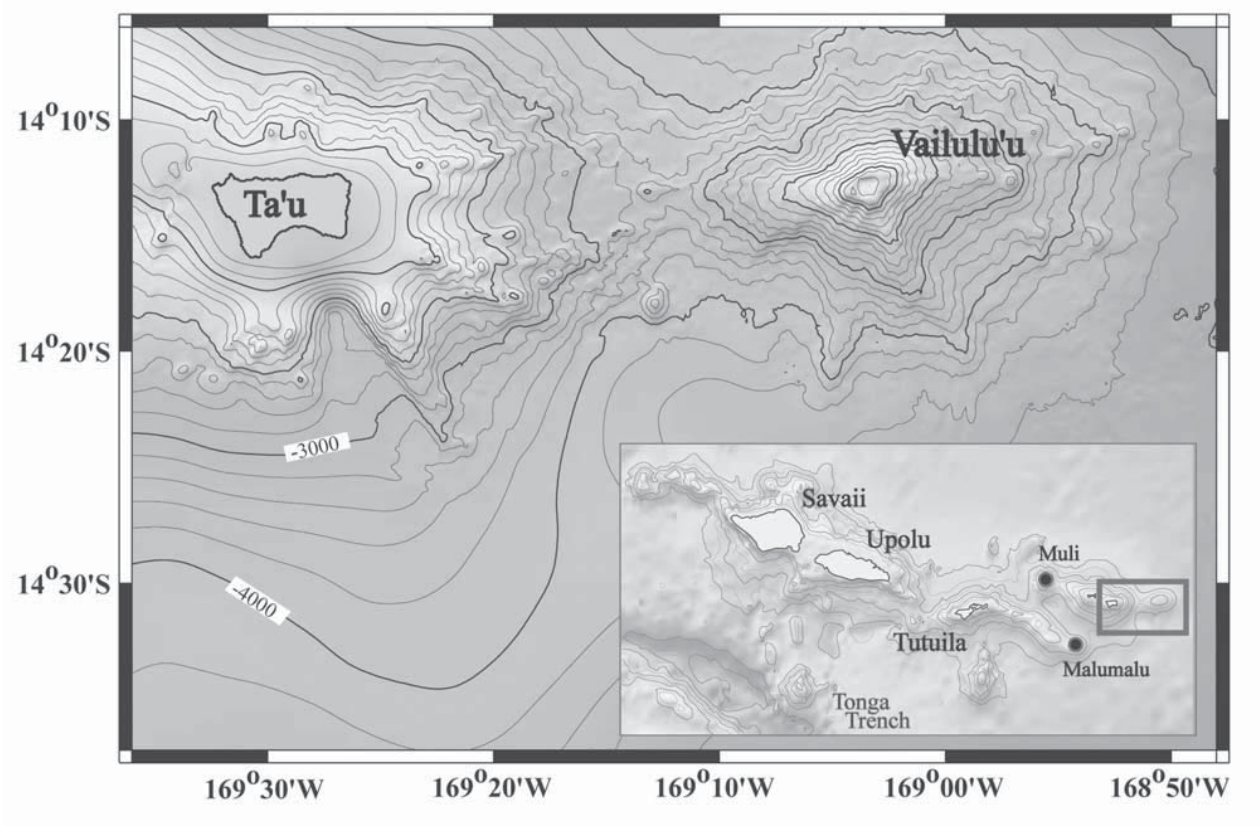

Figure 1. Map showing the location of Vailulu'u volcano with respect to the other volcanic centers of the Samoan hot spot chain. Vailulu'u volcano is 4400 m high and is "connected" to Ta'u island by a deep volcanic ridge. The volcano is 40 km in diameter and located 45 km east of Ta'u. The morphology is marked by a prominent summit caldera 2 km wide by 400 m deep, three volcanic rift zones, several debris avalanche scarps, and numerous debris avalanche run-out deposits [*Hart et al.*, 2000]. See color version of this figure in the HTML.

tracer release in the bottom of the crater, followed by 4 days of mapping with a CTD/F, in tow-yo mode (*Kim et al.* [1994] were the first to successfully utilize a dye release to map the small-scale (∼10 m) length characteristics of an individual hot smoker). This experiment enables us to constrain the total mass and thermal fluxes from the crater; future experiments designed to measure in situ high-temperature fluxes will then enable a determination of the partitioning of fluxes between high-temperature and diffuse flows.

2. Experimental Details

[5] On 3 April 2001, we released a 20 kg point source charge of fluorescein dye near the bottom of Vailulu'u crater (Figure 2). The fluorescein was dissolved in surface seawater to a specific density of ∼1.13, and the density of this solution was then adjusted with isopropanol and fresh water to be 1.4 per mil heavier than the ambient water at release depth. The final volume of solution was 180 L. The density adjustment ensured that any upward dispersal was a hydrothermal entrainment effect, not a dye buoyancy effect. The dye was contained in a rubberized bladder bag, with a 4.5 cm outlet secured by a 4-hour galvanic link (after 4 hours in situ, there may have been some residual thermal buoyancy, as the dye solution was at air temperature when the bag was filled; any residual buoyancy would be rapidly dissipated by entrainment during release). The bag was deployed in free-fall mode, with an anchor, 30 m of tether and glass ball floats attached directly to the bag. The bag was under compression provided by flexible PVC plates strapped to both sides of the bag. We are confident that the bag dropped vertically, because four hydrophones dropped the year previously, with similar moorings, were known to have landed within 35–55 m of the surface drop location by subsequent acoustic ranging on them. Given that the drop site (in 975 m of water) was on the gently sloping north edge of the crater floor, a lateral uncertainty of 40 m corresponds to a vertical uncertainty of ±6m.

[6] The release time and its uncertainty are estimated as 4.5 ± 1.5 hours, as follows: (1) several of the galvanic links were tested in the lab in seawater at 5.3°C, and releases of 4–5 hours were observed; and (2) first detection of dye in the water column was noted at 6 hours postbag deployment. The effective release depth is somewhat more uncertain; while the bottom depth is well constrained at 975 ± 6 m, leading to a bag depth of 945 ± 6 m, the density of the ejected dye solution will depend on the amount of ambient water entrained into the dye during release. With an orifice diameter of 4.5 cm, and an estimated average exit velocity

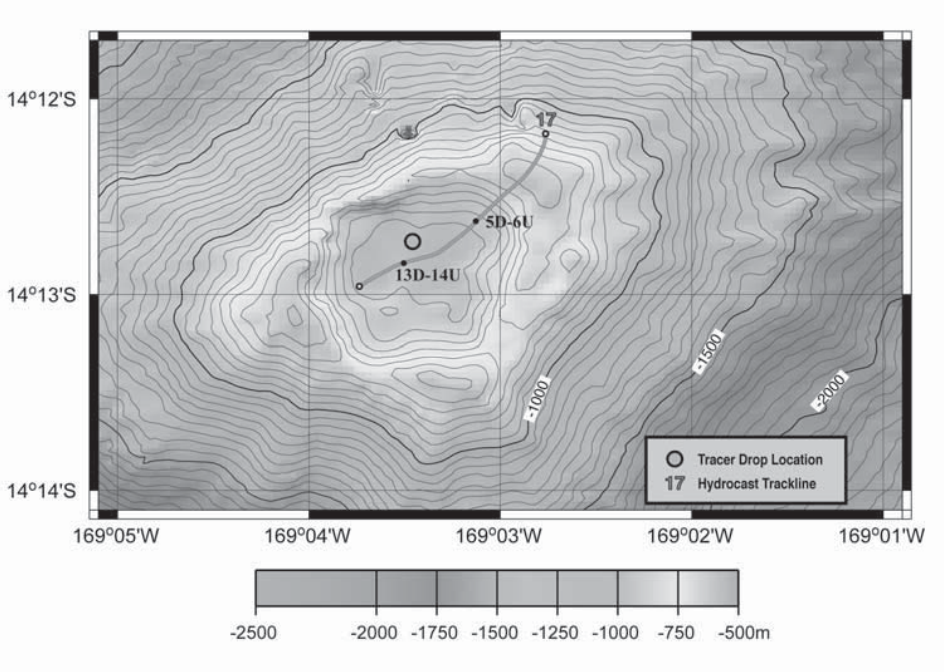

Figure 2. The summit crater of Vailulu'u volcano has a flat "lava lake" floor at 1000 m water depth, a rim with peaks rising to 590 m, and three breaches at 730, 770, and 795 m. The lower 205 m of the crater is thus completely enclosed. The point source dye release location is indicated at the northern edge of the crater floor at a water depth of 945 m (30 m above the floor). Also shown is the track line for tow-yo leg 17, as discussed in text. See color version of this figure in the HTML.

of $\sim$1 m s^{-1}, the entrainment ratio is estimated to be 10^3–10^4 (from a model for a nonbuoyant jet [*Turner*, 1973]). Given this range of entrainment ratios, the initial 1.4 per mil density excess, and the gradient of potential density near the crater bottom, the dye solution after dilution might sink from 3 to 30 m below the orifice depth. These uncertainties will be carried into the data analysis below.

[7] The resulting dye pool was surveyed by CTD/fluorimeter tow-yos from the U.S. Coast Guard icebreaker *Polar Sea*; first detection of the dye was 6 hours after deployment, and the last profile before ship departure was 91 hours after deployment. The Chelsea^{Aquatracker} III fluorimeter had been calibrated in the lab with a series of 16 gravimetric fluorescein solutions ranging in concentration from 150 pg g^{-1} (picograms of dye per gram of water) to 1 μg g^{-1} (micrograms of dye per gram of water); the voltage output of the fluorimeter was precisely log-log linear over a range from 1000 pg g^{-1} to 0.5 μg g^{-1}. The equation of this line was: concentration (in grams of dye per gram of water) = $10^{(voltage-10.58)}$; the detection limit is 26 pg g^{-1}. Background readings in the ambient water of the crater prior to release were very clean (<26.9 pg g^{-1}).

3. Survey Results

[8] Dispersal of the dye pool was monitored with over 150 casts, during 19 tow-yo legs inside the crater. Locations of these legs are not shown in Figure 2, for reasons of clarity, but are given by H. Staudigel et al. (unpublished manuscript, 2002). Most of the legs were oriented along NE-SW "free-drift" lines, as the ship captain was unwilling to run the CTD/F while underway (!). Surveying began immediately after deployment of the dye bag. Thin schlieren of dye were detected some 160 m NW of the drop location, at 815 m depth, just 6 hours after the drop. These schlieren, typically 1–3 m thick and of low concentration (<35 pg g^{-1}), were encountered numerous times in the 740–840 m depth range over the next 30 hours. We did not encounter them higher in the water column so they are clearly related to postrelease dispersion, perhaps by entrainment in small buoyant plumes rising from the crater bottom. In some cases, these schlieren were traceable over hundreds of m from one tow-yo cast to another; in other cases, they appear to be isolated encounters. In no case during the surveying did we see dye above 600 m, nor on any of the casts outside the crater at the levels of the breaches.

[9] Unfortunately, none of the early survey casts reached below 890 m depth, so we were unable to delineate the early stages of dispersion of the main dye pool (different from the schlieren mentioned above). The pool was first detected on cast 17-5D (leg 17, downcast 5D), 39 hours after bag deployment, and 670 m from the drop site. Figure 3 shows the outline of the pool during this leg; the dye "peak" ranges from 870 m to 920 m depth (release depth was >939 m; see above), with peak concentrations of 75–2700 pg g^{-1}. The southern edge of the pool is sharply constrained between casts 17-12U and 17-13D. This "edge" is only 190 m from the drop location, so the dye is clearly not dispersing uniformly in all directions but is being rather strongly advected to the NE from the drop site. The location of

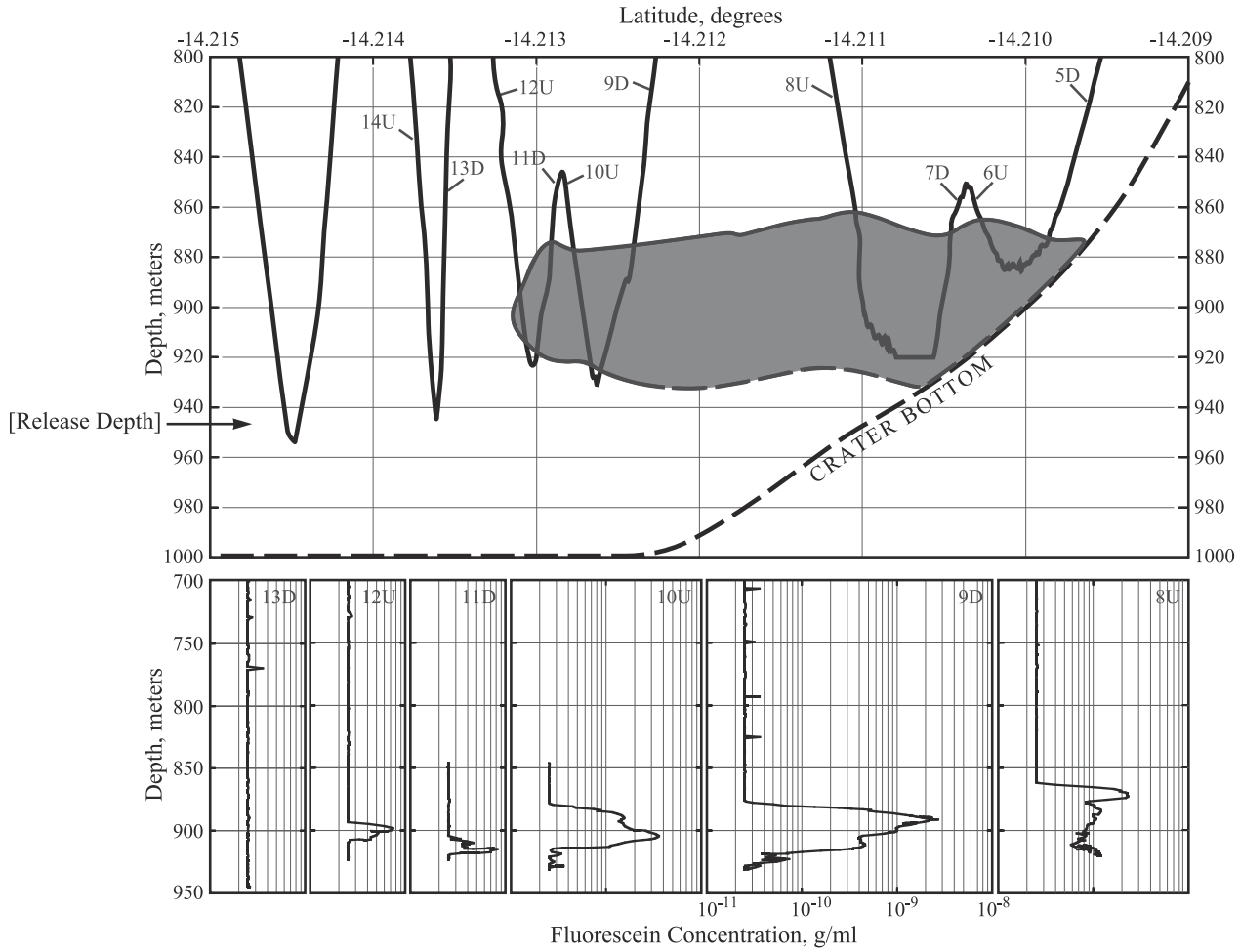

Figure 3. An outline of the dye pool from tow-yo leg 17, 39 hours after dye bag deployment. The pool has already spread laterally by 400 m, dispersed vertically into a 50 m layer, and the layer has been advected upward by some 45 m relative to the nominal release depth (945 m). The tow-yo track (see Figure 2) passed 170 m south of the release point at cast 13D (see Figure 2) where no dye was detected; however, dye was clearly seen on cast 12U. The dye is thus not spreading purely radially but is also being advected to the E-SE along the crater wall. A second profile through this area 4 hours later detected dye 200 m farther south, providing a strong constraint on horizontal dispersion velocities. The dye pool outline is drawn through a depth of 875m on cast 17-11D to accommodate several small secondary peaks not well seen on the profile in this figure.

dye at 17-5D shows that net horizontal velocities reached at least 0.56 cm s^{-1} (20 m h^{-1}).

[10] It is clear from Figure 3 that the dye "peaks" are not strictly Gaussian in shape, unlike the usual case in open ocean tracer experiments [*Ledwell et al.*, 1998; *Ledwell and Hickey*, 1995]. In particular, cast 17-8U shows a dye peak of 230 pg g^{-1} at 870 m, underlain by a layer of rather constant dye concentration of about 100 pg g^{-1} and some 45 m in vertical thickness. While Gaussian-type peaks were frequently encountered on other legs, a wide variety of other peak shapes were also observed. Figure 4 shows a sampling of these: 18-32U is fairly classic, 25-1D shows again, as in 17-8U (Figure 3), a peak overlying a well-mixed layer, 25-4U shows a broad double peak and 18-34U shows an intense triple peak. The multiple peaks are likely caused by dense water from outside being advected into the crater through the breaches, sinking, and spreading laterally along isopycnals, thereby "splitting" the dye peaks.

4. Diapycnal Eddy Diffusivities

[11] In order to determine the vertical diapycnal or eddy diffusivity from our data, given the erratic peak shapes, we feel it is inappropriate to use the curve-fitting method of *Ledwell et al.* [1998]. Rather, we choose to use a simple diffusion rule of thumb, employing a single measurement of the peak width at 37% ($1/e$) of the peak height. This is "low" enough on the various peaks to encompass much of the dye that constitutes the peaks. Of the 31 legs that intersected the dye layer, 22 penetrated far enough to delimit both top and bottom boundaries of the dye peak at a 37% height definition (see Table 1). We will analyze these

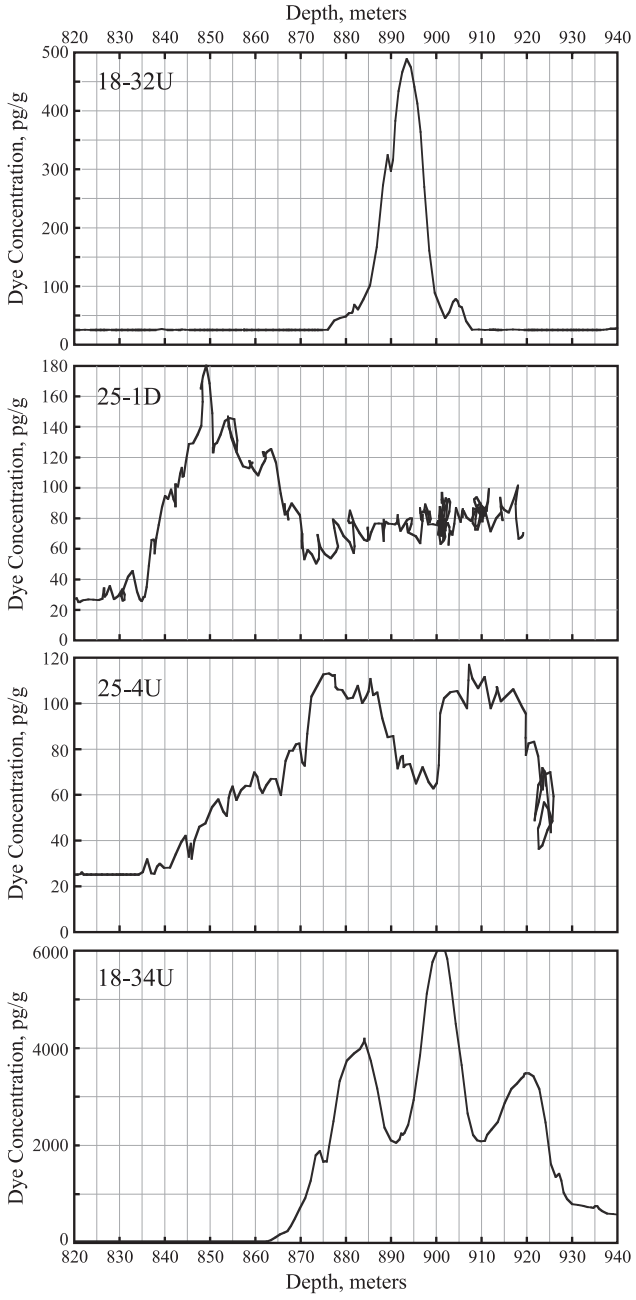

Figure 4. Examples of different "peak shapes" for profiles through the fluorescein dye pool. 18-32U shows a fairly classic "Gaussian" peak, on a cast just 260 m from the drop location. 25-1D shows a peak underlain by a layer of constant concentration, 470 m from drop, while 25-4U shows a double peak, 440 m from drop. 18-34U shows a triple peak, with quite high dye concentrations, 330 m from drop. 18-32U and 18-34U are only 130 m from each other, and 12 min apart in time, indicating the rather chaotic nature of the dispersal process. The jagged nature of parts of the Leg 25 profiles reflects periods when the winch was stopped.

profiles as if the vertical dispersion of the dye follows a "Fickian" diffusion model, and we will derive a "rule of thumb" as follows:

[12] For a thin but finite layer of water carrying passive dye tracer initially of uniform concentration, emplaced horizontally into water with zero dye concentration, the solution of Fick's second law gives [*Jaeger*, 1968]

$$C_z/C_o = \frac{1}{2}\left[erf\left(\frac{Z+A}{2\sqrt{Kt}}\right) - erf\left(\frac{Z-A}{2\sqrt{Kt}}\right)\right] \quad (1)$$

where C_0 is the initial dye concentration, Z is the vertical distance from the midplane of the layer, A is the half thickness of the layer, K is the diffusivity (eddy or diapycnal), and t is time. Note that K is not a measure of the molecular diffusion of dye but relates to the dispersion of the passive dye tracer produced by "microconvection" of the water (molecular diffusion in water is many orders of magnitude slower than this eddy diffusion). The model for equation (1) is obviously a simplification, insofar as the dye was released as a point source; as shown earlier, however, the dye dispersed horizontally fairly rapidly relative to the vertical dispersion, so this approximation will suffice to first order.

[13] The concentration C_c at the center of the layer ($Z = 0$) is then

$$C_c/C_o = \mathrm{erf}\left(\frac{A}{2\sqrt{Kt}}\right). \quad (2)$$

For small values of x, erf(x) = 1.128(x), and

$$C_c/C_o = \frac{1.128A}{2\sqrt{Kt}}. \quad (3)$$

For distances outside the initial layer greater than $\sim 2A$, equation (1) can be approximated as

$$C_z/C_o = \left(\frac{A}{\sqrt{\pi Kt}}\right)\exp\left(-\frac{Z^2}{4Kt}\right). \quad (4)$$

Then the ratio of the concentration outside at distance Z to that at the center of the layer is, from equations (3) and (4),

$$C_z/C_c = \exp\left(-\frac{Z^2}{4\mathrm{Kt}}\right). \quad (5)$$

For $C_z/C_c = 0.368$ (=1/e), we derive the "rule of thumb":

$$K = \sigma^2/4t, \quad (6)$$

where σ is the half-layer thickness at 37% peak height.

[14] For the 22 profiles where both of the 37% limits of the dye layer could be determined, we derived values for σ, and these are plotted (as σ^2) against elapsed time in Figure 5a. The slope of a line on this plot gives, from equation (6), a value for K, the diapycnal diffusivity. Clearly, the data do not define a single line, suggesting a departure of K from a simple diffusion model (clear from the peak shapes in Figure 4), and probably a variation of K from place to place in the crater. As might be expected, there is a fair

Table 1. Fluorimeter Tow-Yo Data[a]

Cast	Latitude	Longitude	Distance to Drop, m	Day of Year	Elapsed Days	Depth of Cast, m	Depth of Layer,[b] m	Peak Depth,[c] m	Peak Concentration, pg g^{-1}	Sigma[d]	Sigma Squared
Bag Drop	−14.21207	190.94263	0	94.170	0						
17-6U	−14.21019	190.94816	636	95.792	1.622	885	870	878	91	9.0	81
17-7D	−14.21053	190.94782	589	95.794	1.624	920	877	908	420		
17-8U	−14.21102	190.94734	524	95.795	1.625	920	865	878	230	13.5	182
17-9D	−14.21246	190.94550	315	95.805	1.635	930	886	892	2,700	7.0	49
17-10U	−14.21271	190.94521	289	95.808	1.638	930	888	905	360	11.8	139
17-11D	−14.21299	190.94480	256	95.809	1.639	923	909	915	83	4.8	23
17-12U	−14.21309	190.94462	244	95.810	1.640	923	895	899	74	5.5	30
18-29D	−14.21420	190.94251	233	95.987	1.817	952	939	941	79	1.6	3
18-31D	−14.21405	190.94303	222	95.990	1.820	952	902	907	98	7.5	56
18-32U	−14.21406	190.94327	230	95.993	1.823	960	887	894	490	7.0	49
18-33D	−14.21413	190.94434	294	95.999	1.829	954	893	904	17,800	16	256
18-34U	−14.21420	190.94437	302	96.001	1.831	954	874	902	6,200	25	625
19-8D	−14.21144	190.94174	118	96.168	1.998	943	924	931	42	9.0	81
19-9U	−14.21144	190.94166	126	96.169	1.999	941	925	929	47	7.0	49
23-3D	−14.20879	190.94428	410	97.559	3.389	832	751	764	39		
23-5D	−14.21121	190.94213	112	97.569	3.399	918	859	878	166	25	625
23-6U	−14.21171	190.94171	106	97.571	3.401	918	865	894	162	29	841
23-7D	−14.21322	190.94044	264	97.576	3.406	918	887	925	510		
23-9U	−14.21443	190.93944	428	97.581	3.411	938	838	890	320	52	2704
24-4D	−14.20903	190.94431	388	97.677	3.507	804	767	795	48		
24-5U	−14.20937	190.94401	340	97.678	3.508	804	755	767	62		
25-1D	−14.21143	190.94725	507	97.734	3.563	919	840	878	178	38	1444
25-2U	−14.21273	190.94658	434	97.737	3.567	919	854	887	138	33	1089
25-3D	−14.21376	190.94603	413	97.740	3.570	923	864	883	158	30	900
25-4U	−14.21455	190.94562	424	97.741	3.571	923	856	894	117	36	1296
27-1D	−14.21509	190.94584	483	97.964	3.794	920	851	889	240	39	1521
27-2U	−14.21560	190.94582	522	97.975	3.805	920	837	885	250	48	2304

[a]Locations and times refer to the CTD location at the peak of the dye layer.
[b]Depth of layer is to the point at 37% of peak height.
[c]Peak depth is depth to actual peak (if single) or to the midpoint between the 37% concentrations on top and bottom of layer.
[d]Sigma is the half thickness of the dye layer at 37% of the peak concentration.

correlation (not shown) between the values of σ^2 and the gradient in potential density, with faster dispersion correlating with smaller density gradients (the buoyancy frequency at 800–960 m in the crater ranged from 0.11 to 0.55 cycles per hour, averaging 0.37 cph). The data of Figure 5a were fit with a 2-error regression [*York*, 1966], leading to $K = 21.1 \pm 2.7$ cm^2 s^{-1} ($\pm 1\sigma$). Uncertainties in the thickness of the dye layer were individually assigned to each point, as estimated from the nature of the profiles (e.g., Figures 3 and 4). We did not constrain the regression to go through the release time (0.2 ± 0.1 days), as many of the legs were distant from the drop site and the dye obviously did not immediately disperse horizontally into a crater-wide layer. In effect, the data cluster at 1.6–2.0 days defines an initial condition for the dye layer. In addition to the formal 1σ uncertainty stated above, approximate extreme bounds to the data are also indicated on Figure 5a; these limits are $K > 9$ cm^2 s^{-1} and <38 cm^2 s^{-1}. The vertical dispersion of dye is clearly diapycnal, as the leading top edge of the dye layer is observed to progressively move into lower density water (at a rate ranging from 0.002 to 0.005 kg m^{-3} d^{-1}).

[15] These diapycnal diffusivities are significantly greater ($100\times$) than those observed in open oceanic environments. For example, *Ledwell et al.* [1998] measured a value for K of 0.17 cm^2 s^{-1} just below the pycnocline in the North Atlantic, and a value of 0.29 cm^2 s^{-1} was measured at 790 m depth in the central part of the Santa Monica basin [*Ledwell and Watson*, 1991]. However, in oceanic areas where rough topography or boundary effects are dominant, values for K in the range of 3–25 cm^2 s^{-1}, similar to ours, have been measured (14–25 cm^2 s^{-1}, near bottom on Georges Bank [*Houghton and Ho*, 2001]; 3–8 cm^2 s^{-1}, at 4000–4500 m on the flank of the MAR [*Ledwell et al.*, 2000]; 10 cm^2 s^{-1}, near the walls of the Santa Cruz basin [*Ledwell and Bratkovich*, 1995]).

5. Vertical Advection Velocities

[16] It is apparent from the data in Table 1 that the dye pool is not only thickening by diapycnal diffusivity, but the dye layer overall also has an upward drift due, presumably, to vertical advection currents. The easiest way to deconvolve the diffusivity from the advection is by using the layer thickness to determine K (as was done above), and to use the depth of the peak of dye concentration to track upward advection; these data are shown in Figure 5b. The principal uncertainty in this approach is determining the peak depth, when the peaks are misshapen as they frequently are (e.g., Figure 4). In these cases, we simply used the midpoint of the 37% limits on the peak width. In Figure 5b, we have used the nominal release time and depth as an initial condition, and regressed the data with the *York* [1966] two-error treatment. Again, errors in peak depth were estimated from the individual profiles and assigned to each point. The release time and depth exert a strong control on the regression; the minimum release time was taken as 3 hours postdeployment (see section 2). The maximum release time was taken as the time of first dye detection (6 hours). The minimum depth (939 m) was derived assuming the final anchor location was 40 m north

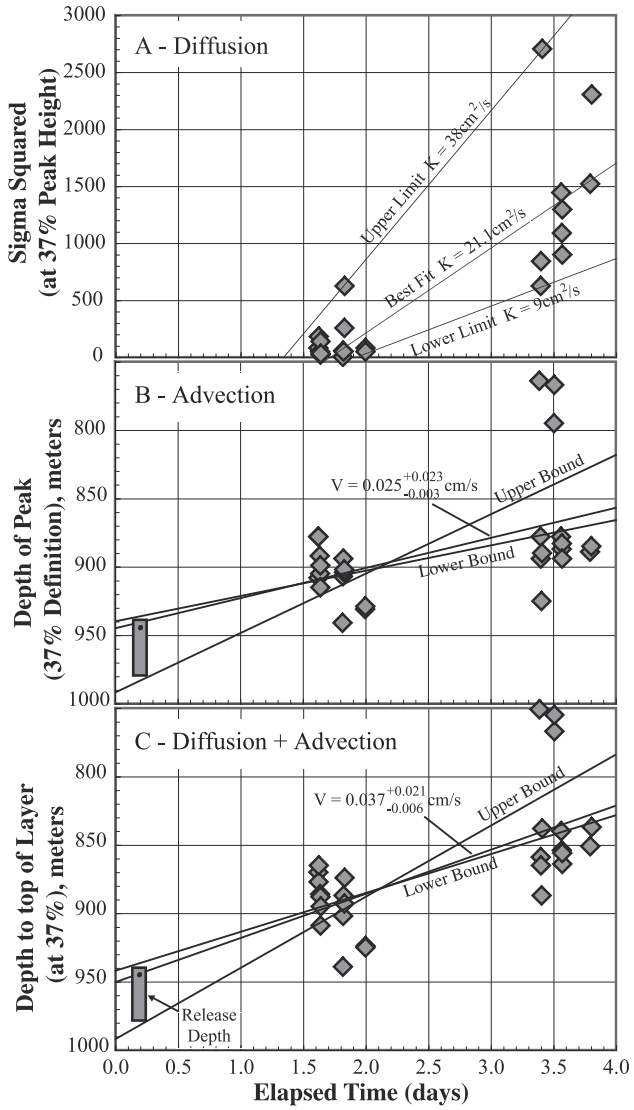

Figure 5. (a) Thickness of the dye layer, measured at 37% of the peak height, versus elapsed days from time of dye drop, for all of the casts which penetrated the dye pool. Bounding lines for $K = 9$ cm^2 s^{-1} and $K = 38$ cm^2 s^{-1} are shown (from equation (6)), along with the best fit line to the data, $K = 21.1 \pm 2.7$ cm^2 s^{-1}. The lines were not constrained to go through the release time (0.25 days), as the point source release took some time to develop into a layer morphology by lateral advection. (b) Depth of the dye peak (defined as the depth midway between the 37% levels on both the upper and lower sides of the dye peak) versus elapsed time. The box shows the uncertainties in the release time and depth. The best fit line, with propagated lower and upper bounds gives $0.025^{+0.023}_{-0.003}$ cm s^{-1}. These data should constrain solely the vertical advection velocity component, independent of the diapycnal diffusion component. (c) Depth of the top of the dye layer, measured at 37% of the peak height, versus elapsed time. The box shows the uncertainties in the release time and depth. The best fit line, with propagated lower and upper bounds, gives $0.037^{+0.021}_{-0.006}$ cm s^{-1}; this line represents the "effective" upward advection, due both to the vertical advection and the upward spreading by diapycnal diffusivity.

of the surface deployment location, and accounting for the 30 m tether line (40 m is the mean uncertainty of the ocean bottom hydrophone locations; see above). The maximum depth (981 m) was set as the actual bottom depth 40 m south of the drop location (to account for a case where the dye density, after extrusion from the bag and local entrainment, was greater than the bottom water density). The nominal "best estimate" time and depth were taken as 4.5 ± 1.5 hours and 945 ± 6 m. This best fit line (Figure 5b) corresponds to a vertical advection velocity of $V = 0.025$ cm s^{-1}. Absolute lower and upper limits were derived by forcing the regression through first the minimum release time and depth (3 hours and 939 m), and then the maximum release time and depth (6 hours and 981 m). These lower and upper limit velocities are 0.022 and 0.048 cm s^{-1}, respectively. Thus we quote the advection velocity from these data as $V = 0.025^{+0.023}_{-0.003}$ cm/s.

[17] We believe the variation in advection velocity observed in Figure 5b is real and reflects variable upwelling rates in different parts of the crater. As a test of this, we note that in two cases there are tow-yo casts from the early and late groups that are geographically coincident. In one of these (18-34U and 25-4U, see Figure 4), the dye peak has moved upward by very little ($\sim$8 m) in 1.7 days, the peak has decreased in intensity by a factor of 50, and the shape has changed from a triple peak to a double peak. In the other case (19-8D and 23-6U, Table 1), the dye peak increased in intensity by a factor of 4 and moved upward by 37 m in 1.4 days ($V = 0.031$ cm s^{-1}). Of course, there are major horizontal advections occurring at the same time, and we don't mean to imply that a single parcel in one location is simply rising.

[18] If the vertical "advected" motion of the upper surface of the dye layer was misinterpreted as layer broadening due to diapycnal diffusivity, the apparent K values so derived (40–320 cm^2 s^{-1}) would grossly over-estimate the true diffusivities (9–38 cm^2 s^{-1}, see Figure 5a). In terms of overall mass transport then, clearly the advected field is dominant relative to the diffusive field. We may estimate an "apparent" vertical velocity field which combines both the advected and diffusive components by looking at the vertical motion of the upper surface of the dye layer; Figure 5c (while diffusivity does not have velocity units but scales as velocity x distance, the movement of a diffusive front may be treated to first order as a velocity because the diffusion scale length is of the same order as the crater depth, over the 3–4 day residence time of water in the crater; see below). We regressed the data of Figure 5c in the same fashion as described above. Using the best estimates for release time and depth, we obtain $V = 0.0369 \pm 0.0076$ cm s^{-1}. Lower and upper bounds are determined by forcing the data through the extreme limits on release time and depth; these two regressions give $V = 0.0344 \pm 0.0033$ and 0.0538 ± 0.0041 cm s^{-1}. Thus as extreme bounds we take $0.0344 - 0.0033 = 0.0311$ cm s^{-1} and $0.538 + 0.0041 = 0.0579$ cm s^{-1}. The final "apparent" vertical advection velocity then may be quoted as cm s^{-1}. This velocity may be compared with that derived for advection alone from Figure 5a, $V = 0.025$ cm s^{-1}. Thus the advected field carries some 70% of the mass flux. This distinction will become important in our discussion below regarding heat and chemical fluxes.

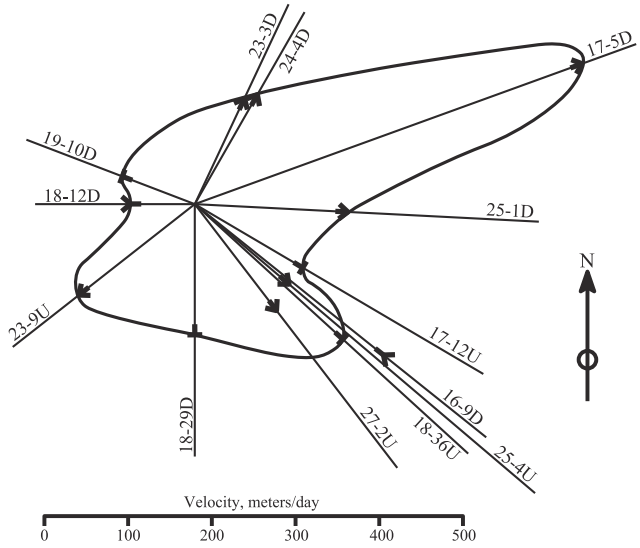

Figure 6. Horizontal dispersion velocities, as a function of azimuth, for various casts that constrain the ''edges'' of the dye pool. Distance limits derived from various casts have been divided by the corresponding times to obtain velocity vectors, where the length of the vector is proportional to velocity. The ''T'' symbols are places where the edge of the dye pool was well constrained, with the distance from the dye origin signifying velocities in meters per day. Outward facing arrows are lower limits, and inward facing arrows are upper limits, to the horizontal velocities. The enclosing outline is drawn to be consistent with the various velocity limits, and shows that the dye pool is spreading to the northeast much more rapidly than to the west (more than 500 m d^{-1} versus less than 80 m d^{-1}).

[19] To accurately define a mean upwelling rate for the crater as a whole would require full coverage of a planar cross section of the crater; this must await a more thorough tracer experiment. There obviously needs to be a ''return'' flow to recharge the deep waters of the crater, as argued by *Staudigel et al.* [2001, also unpublished manuscript, 2002]; this is provided by the colder and denser outside waters that are advected in through the breaches (see later discussion). This colder water is believed to flow down the inner crater walls as boundary layer flows and probably does not occupy much of the area of a planar cross section of the crater. Correlation of sporadic external cold upwelling events recorded on temperature loggers on the crater rim and on the bottom of the crater define transit times of only a few hours, implying sinking velocities of 5 cm s^{-1}. These velocities are at least 100 times higher than the vertical advection velocities detailed above, confirming the likelihood that the return flow is restricted to the near-crater-wall zone. Similar gravity flow velocities were reported on the sloping walls of Lake Geneva [*Fer and Lemmin*, 2001].

6. Horizontal Advection Velocities

[20] From the various intersections of the dye pool during the CTD/F tow-yos, we are able to constrain the horizontal advection velocities; these constraints are shown on a ''current'' map in Figure 6. In some cases, tight limits are obtained, in other cases either upper or lower limits are set. The maximum observed velocity is to the NE, and is in excess of 500 m d^{-1}; minimum velocities are to the west at about 80–100 m d^{-1}. Velocities to the south and southeast are intermediate, in the range 140–230 m d^{-1}. Clearly more detailed work is required to fully delineate the horizontal current field, and its possible time variation. In any event, these velocities are sufficiently high to distribute a tracer throughout most of the crater at the 800 m level in only 3–6 days.

7. Dye Inventory

[21] Given the lack of dynamic positioning capability on the ship, we were unable to fully delineate the extremes of the dye pool over time, particularly in areas near the crater walls. We consider here the observations relative to a theoretical ''crater-wide'' dye budget to assess the completeness of lateral spreading. We calculate the peak dye concentration expected, as a function of layer thickness, from equations (3) and (4); for a peak width (2σ) measured at 37% of peak height, 85% of the dye will be within $\pm 1\sigma$. Over the depth interval of interest (830–900 m), the volume of water per meter of depth interval varies only slightly, with a mean value of 1.9×10^6 m^3; 20 kg of fluorescein (86% purity), initially distributed over a 2 m layer, would give a peak concentration of 4700 pg g^{-1}. Figure 7 shows the expected concentration at the peak, as a function of σ, in comparison with the observed data. The early casts are distributed widely on both sides of the theoretical curve, indicating uneven dispersion of dye with respect to the cast locations. The later casts fall closer to the theoretical budget, though several show a tendency toward high concentrations, indicating the dye pool has still not dispersed quite evenly across the crater. This is consistent with the horizontal

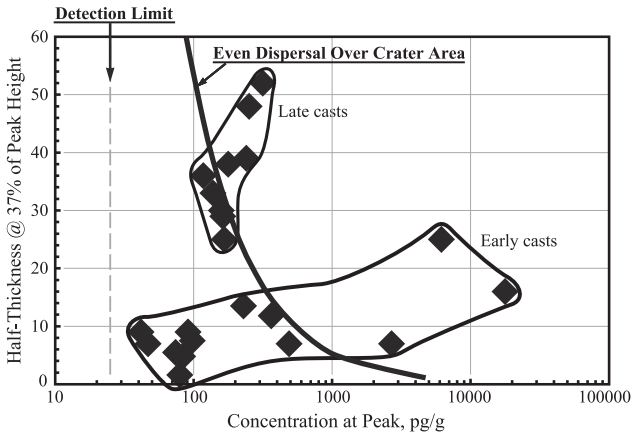

Figure 7. Comparison of observed dye layer thicknesses and peak concentrations with a theoretical diffusion model whereby 85% of the dye is contained in a layer bounded between the 37% peak height points, and assumed to be evenly dispersed over the whole crater area at a nominal depth of 865m. The two fields enclose the early casts (days 1.6–2.0) and the late casts (days 3.4–3.8) and suggest that the later casts come close to a even dispersal budget while the early casts are clearly made before the dye pool was fully dispersed across the full crater area.

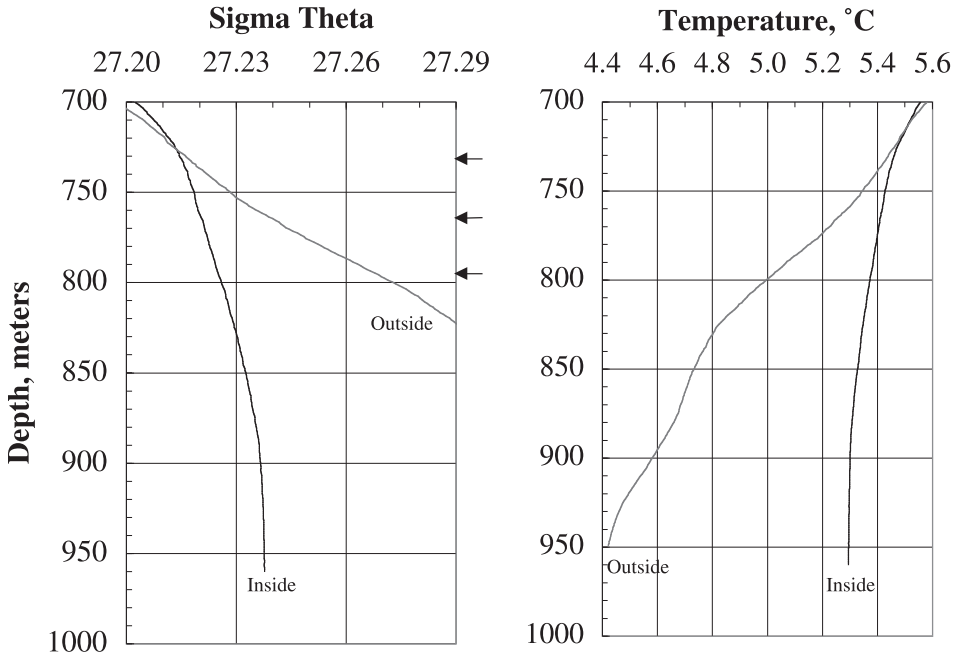

Figure 8. Average potential temperature and potential density profiles for CTD casts made both inside and outside of the crater, during the 2001 cruise. The inside average is composed of 83 individual casts, the outside average is composed of 22 individual casts. For both temperature and density, the profiles diverge or bifurcate at a depth of 730 m, with the outside water being colder and denser below the bifurcation depth. The arrows show the depths of the three breaches (730, 765, and 795 m).

current limits established above, which suggest that, particularly to the W-SW, it could take 5–6 days to reach the crater walls.

8. Mass Fluxes

[22] It is apparent from the average temperature and potential density profiles from inside and outside the crater (Figure 8) that water column properties begin to diverge (bifurcate) strongly below about 730 m depth. More than 95% of the cross-sectional breach area lies above 730 m, so it is clear that the water column has to be very well "protected" from the outside (<5% of breach area) before the crater begins to feel isolation. For the various flux calculations below, we assume that once water parcels rising from the crater reach 730 m, they are rapidly swept away by the cross flow from outside the crater.

[23] The horizontal cross-sectional area of the crater at 830m (mean depth of dye layer at 4 days), is 2.5×10^6 m^2. With an average "apparent" (advection plus diffusion) vertical velocity of $0.037^{+0.021}_{-0.006}$ cm s^{-1}, the implied export of water from the crater is $8.0^{+4.6}_{-1.3} \times 10^7$ m^3 d^{-1} (assuming as discussed earlier that the recharge area is small relative to the export area). With a total crater volume below 830 m of 2.55×10^8 m^3, this export rate amounts to 31% of the crater water per day, or approximately a $3.2^{+0.6}_{-1.2}$ day "turnover" time. Note that while all of this export water is "tagged" with a hydrothermal signature, clearly not all of it has passed through the subsurface hydrothermal system.

[24] H. Staudigel et al. (unpublished manuscript, 2002) calculated an import flux, based on the observation from Figure 8 that the water outside the crater below 730m is heavier than that inside the crater. Using a model adapted from *Whitehead* [1998] for density-driven flow over a sill (in this case, through a notch), the import flux of outside water into the crater was determined to be 1.3×10^8 m^3 d^{-1}. While near the upper bound of the export flux determined above of $0.67–1.26 \times 10^8$ m^3 d^{-1}, the agreement is excellent, given two factors. First, the import model neglects turbulence and frictional effects and will thus tend to overestimate the import flux. Second, only the water advected in below 760 m (Figure 8) will sink to the bottom of the crater; water between 760 and 730 m bifurcation depth will spread laterally along isopycnals without reaching the crater bottom. In effect, some of the imported water is not available at the depths where the export flux from the dye experiment was determined, so we cannot expect the calculated import and export fluxes to be sensibly balanced. The "turnover" time calculated from the import flux, based on the volume of water in the crater below the 730 m bifurcation depth (5.4×10^8 m^3), is 4.1 days, comparable to the 3.2-day "turnover" time calculated for deep crater water from the dye experiment.

9. Thermal Fluxes

[25] As noted above (Figure 8), the inside and outside temperature profiles bifurcate at ~730 m, and the temperature difference at 795 m (depth of the deepest breach) is 0.35°C; the integrated temperature excess over this depth range is 0.153°C. Exporting $8.0^{+4.6}_{-1.3} \times 10^7$ m^3 d^{-1} of water with an excess heat content of 0.66×10^6 J m^{-3} (0.153°C × 4.3 J g^{-1}) gives a thermal power of 610^{+350}_{-100} MW (or about 250 W m^{-2} of area at 830 m). This is a large power output

when compared to active hydrothermal fields on spreading ridges, which are typically about 75 ± 45 MW km^{-1} of ridge length (diffuse plus discrete flows [*Baker et al.*, 1996]). A survey of individual hot smokers on the Juan de Fuca ridge showed outputs up to 50 MW, but the average of 36 vents was ~6 MW [*Bemis et al.*, 1993]. The crater output is more comparable to the overall output of the TAG field (both diffuse and discrete flows), which has been estimated at 780–2513 MW [*Schulz and Elderfield*, 1997], or the 600 MW output of the Main Endeavor vent field (over an area of 0.3 km^2) reported by *Yoerger et al.* [2001]. In any event, we believe our power calculation is reasonably conservative.

[26] How much basalt must be cooled to supply the 610 MW of power output? The total heat content of basalt magma (enthalpy of fusion plus specific heat content from 1250°C) is 6.6×10^9 J m^{-3}; if the basalt "layer" being mined for heat has an area equivalent to that of the crater floor up to the 900m depth level (1.8×10^6 m^2), then 1.6 m of basalt per year must be cooled to supply the hydrothermal power being exported from the crater. If the earthquake swarm observed at Vailulu'u in 1995 signaled a magmatic intrusive event beneath the crater, and if a magma lens of even 30–50 m was intruded, then the current state of hydrothermal activity at Vailulu'u could, from this one intrusion alone, continue unabated for several more decades, given adequate access of water to the magmatic system.

10. Chemical Fluxes

[27] The average Mn content of water in the crater below 700 m is 3.0 ± 0.2 ppb (H. Staudigel et al., unpublished manuscript, 2002). With the water flux calculated above of $8.0^{+4.6}_{-1.3} \times 10^7$ m^3 d^{-1}, the Mn export flux is 240^{+140}_{-40} kg d^{-1}. This is significantly larger than the Mn flux from a typical mid-ocean ridge hot smoker of about 30 kg d^{-1} (though this flux varies widely), and is also ~8 times the Mn flux from the Broken Spur vent field [*Murton et al.*, 1999]. The Mn/heat ratio is 4.7 ng J^{-1}, which is considerably lower than ridge crest hydrothermal settings. For example, hot smokers have Mn/Q ratios of 50–60 ng J^{-1} [*Von Damm*, 1990]; low-temperature diffuse flow fluids have Mn/Q ratios of 6–200 ng J^{-1} [*Baker et al.*, 1993; *Massoth et al.*, 1994; *Wheat and Mottl*, 1994], and steady state plumes range from 20 to 55 ng J^{-1} [*Baker et al.*, 1993; *Massoth et al.*, 1994]. However, event plumes tend to be lower, with Mn/Q ratios of 3–8 ng J^{-1} [*Lupton et al.*, 2000], as are high-temperature phase-separated fluids, with values at two localities of 5.5 and 6.6 ng J^{-1} [*Von Damm et al.*, 1997; *Massoth et al.*, 1989]. We believe the low Mn/Q ratio in Vailulu'u crater indicates the operation of a phase separation process (supported as well by the high He/Mn ratios reported by H. Staudigel et al. (unpublished manuscript, 2002)).

[28] This quantity of Mn could be supplied by mining about a 1 cm layer of basalt per year, compared to the 1.6 m of rock needed to supply the heat flux. In other words, after a parcel of rock has been completely cooled, <0.6% of its Mn has been removed. This is essentially a water/rock ratio, and can also be derived more directly by comparing the Mn/heat ratio of rock to that of the water in the crater. Vailulu'u basalt averages 1355 ppm Mn, and the total heat content of magma is 2200 J g^{-1}. The crater water averages 3 ppb Mn, and, with an average excess temperature of 0.153°C, contains 0.64 J g^{-1} of heat. The Mn/heat ratio of rock is thus 616 ng J^{-1} and that of the water is 4.7 ng J^{-1}; the effective water/rock ratio from the Mn budget is thus 616/4.7 ~ 130.

11. Summary

[29] The results from this tracer release experiment in an active submarine hydrothermal system provide the following constraints for the active summit crater of Vailulu'u volcano, Samoa. We emphasize that these findings strictly apply only during the time period of the experiment, and that the quoted uncertainties are propagated solely from the observations. Obviously, these uncertainties need not include aspects of this chaotic hydrothermal system that were not captured during the experiment:

[30] • Horizontal advection velocity ranges from 80 to 500 m d^{-1} (0.09 to 0.58 cm s^{-1}).

[31] • Vertical advection velocity is $0.025^{+0.023}_{-0.003}$ cm s^{-1}.

[32] • Vertical diapycnal (eddy) diffusivity is 21.1 ± 2.7 cm^2 s^{-1}.

[33] • Water mass output from crater is $8.0^{+4.6}_{-1.3} \times 10^7$ m^3 d^{-1}.

[34] • Thermal power output is 610^{+350}_{-100} MW.

[35] • Turnover or residence time of water in the crater is 3–4 days.

[36] • Manganese export is 240^{+140}_{-40} kg d^{-1}.

[37] • Manganese/heat ratio is 4.7 ng J^{-1}.

[38] **Acknowledgments.** We are especially grateful for the help provided by the officers and crew of the *Polar Sea* icebreaker, at a time when the crew was "headed back to the barn", and to the Coast Guard (particularly Phil McGillivary) for making the ship time available. We thank Barrie Walden for technical help in constructing the dye bag and release system and Jim Ledwell for loan of the fluorimeter, consultation on the nuances of tracer release experiments, and a helpful review of the manuscript. Jack Whitehead and Karl Helfrich provided many invaluable GFD tutorials, while Ken Brink and John Toole did the same for PO aspects. The NASA crew we shared ship time with helped keep us up and awake. All travel and support for the experiment were provided by WHOI funds from the C.O. Iselin Chair (to S.R.H.).

References

Baker, E. T., G. J. Massoth, S. L. Walker, and R. W. Embley, A method for quantitatively estimating diffuse and discrete hydrothermal discharge, *Earth Planet. Sci. Lett.*, *118*, 235–249, 1993.

Baker, E. T., Y. J. Chen, and J. P. Morgan, The relationship between near-axis hydrothermal cooling and the spreading rate of mid-ocean ridges, *Earth Planet. Sci. Lett.*, *142*, 137–145, 1996.

Bemis, K. G., R. P. Von Herzen, and M. J. Mottl, Geothermal heat flux from hydrothermal plumes on the Juan de Fuca Ridge, *J. Geophys. Res.*, *98*, 6351–6365, 1993.

Elderfield, H., and A. Schultz, Mid-ocean ridge hydrothermal fluxes and the chemical composition of the ocean, *Annu. Rev. Earth Planet. Sci.*, *24*, 191–224, 1996.

Fer, I., and U. Lemmin, Cascading of water down the sloping sides of a deep lake in winter, *Geophys. Res. Lett.*, *28*, 2093–2096, 2001.

Hart, S. R., et al., Vailulu'u undersea volcano: The new Samoa, *Geochem. Geophys. Geosyst.*, *1*, Paper 2000GC000108, 2000.

Houghton, R. W., and C. Ho, Diapycnal flow through the Georges Bank tidal front: A dye tracer study, *Geophys. Res. Lett.*, *28*, 33–36, 2001.

Jaeger, J. G., Cooling and solidification of igneous rocks, in *Basalts, The Poldervaart Treatise on Rocks of Basaltic Composition*, vol. 2, edited by H. H. Hess and A. Poldervaart, pp. 503–536, Wiley-Interscience, Hoboken, N. J., 1968.

Kim, S. L., L. S. Mullineaux, and K. R. Helfrich, Larval dispersal via entrainment into hydrothermal vent plumes, *J. Geophys. Res.*, *99*, 12,655–12,665, 1994.

Ledwell, J. R., and A. Bratkovich, A tracer study of mixing in the Santa Cruz Basin, *J. Geophys. Res.*, *100*, 20,681–20,704, 1995.

Ledwell, J. R., and B. M. Hickey, Evidence for enhanced boundary mixing in the Santa Monica Basin, *J. Geophys. Res.*, *100*, 20,665–20,679, 1995.

Ledwell, J. R., and A. J. Watson, The Santa Monica Basin tracer experiment: A study of diapycnal and isopycnal mixing, *J. Geophys. Res.*, *96*, 8695–8718, 1991.

Ledwell, J. R., A. J. Watson, and C. S. Law, Mixing of a tracer in the pycnocline, *J. Geophys. Res.*, *103*, 21,499–21,529, 1998.

Ledwell, J. R., E. T. Montgomery, K. L. Polzin, L. C. St. Laurent, R. W. Schmitt, and J. M. Toole, Evidence for enhanced mixing over rough topography in the abyssal ocean, *Nature*, *403*, 179–182, 2000.

Lupton, J. E., E. T. Baker, and G. J. Massoth, Reply to Comment by R. M. Palmer and G. G. J. Ernst on "Helium, heat, and the generation of hydrothermal event plumes at mid-ocean ridges" by J. E. Lupton, E. T. Baker and G. J. Massoth, *Earth Planet. Sci. Lett.*, *180*, 219–222, 2000.

Massoth, G. J., D. A. Butterfield, J. E. Lupton, R. E. McDuff, M. D. Lilley, and I. R. Jonasson, Submarine venting of phase-separated hydrothermal fluids at Axial Volcano, Juan de Fuca Ridge, *Nature*, *340*, 702–705, 1989.

Massoth, G. J., E. T. Baker, J. E. Lupton, R. A. Feely, D. A. Butterfield, K. L. Von Damm, K. K. Roe, and G. T. Lebon, Temporal and spatial variability of hydrothermal manganese and iron at Cleft segment, Juan de Fuca Ridge, *J. Geophys. Res.*, *99*, 4905–4923, 1994.

Murton, B. J., L. J. Redbourn, C. R. German, and E. T. Baker, Sources and fluxes of hydrothermal heat, chemicals and biology within a segment of the Mid-Atlantic Ridge, *Earth Planet. Sci. Lett.*, *171*, 301–317, 1999.

Schultz, A., and H. Elderfield, Controls on the physics and chemistry of seafloor hydrothermal circulation, *Philos. Trans. R. Soc. London, Ser. A*, *355*, 387–425, 1997.

Staudigel, H., S. R. Hart, A. Koppers, C. Constable, R. Workman, M. Kurz, and E. T. Baker, Hydrothermal activity at Vailulu'u Seamount, Samoa, *Eos Trans. AGU*, *82*(47), Fall Meet. Suppl., Abstract OS41A-0435, 2001.

Turner, J. S., *Buoyancy Effects in Fluids*, 368 pp., Cambridge Univ. Press, New York, 1973.

Von Damm, K. L., Seafloor hydrothermal activity: Black smoker chemistry and chimneys, *Annu. Rev. Earth Planet. Sci.*, *18*, 173–204, 1990.

Von Damm, K. L., L. G. Buttermore, S. E. Oosting, A. M. Bray, D. J. Fornari, M. D. Lilley, and W. C. Shanks III, Direct observation of a seafloor "black smoker" from vapor to brine, *Earth Planet. Sci. Lett.*, *149*, 101–111, 1997.

Wheat, C. J., and M. J. Mottl, Hydrothermal circulation, Juan de Fuca Ridge eastern flank: Factors controlling basement water composition, *J. Geophys. Res.*, *99*, 3081–3098, 1994.

Whitehead, J. A., Topographic control of oceanic flows in deep passages and straits, *Rev. Geophys.*, *36*(3), 423–440, 1998.

Yoerger, D. R., A. M. Bradley, F. Stahr, and R. McDuff, Surveying deep-sea hydrothermal vent plumes with the autonomous benthic explorer (ABE), paper presented at 12th International Symposium on Unmanned Untethered Submersible Technology, Autonomous Undersea Syst. Inst., Durham, N.H., 26–29 Aug. 2001.

York, D., Least-squares fitting of a straight line, *Can. J. Phys.*, *44*, 1079–1086, 1966.

A. P. Girard, S. R. Hart, and R. Workman, Woods Hole Oceanographic Institution, Woods Hole, MA 02543, USA. (shart@whoi.edu)

A. A. P. Koppers and H. Staudigel, Scripps Institution of Oceanography, UCSD, La Jolla, CA 92093, USA.